Assessment of Wind Turbine Component Loads Under Yaw-Offset Conditions

Rick Damiani[1], Scott Dana[1], Jennifer Annoni[1], Paul Fleming[1], Jason Roadman[1], Jeroen van Dam[1], and Katherine Dykes[1]

[1]National Renewable Energy Laboratory, Golden, CO, 80401 - USA

Correspondence to: Rick Damiani (rick.damiani@nrel.gov)

Abstract. Renewed interest in yaw control for wind turbine and power plants for wake redirection and load mitigation demands a clear understanding of the effects of running with skewed inflow. In this paper, we investigate the physics of yawed operations, building up the complexity from a simplified analytical treatment to more complex aeroelastic simulations. Results in terms of damage equivalent loads (DELs) and extreme loads under operating, misaligned conditions are compared to data collected from an instrumented, utility-scale wind turbine. The analysis shows that multiple factors are responsible for the DELs of the various components, and that airfoil aerodynamics, elastic characteristics of the rotor, and turbulence intensities are the primary drivers. Both fatigue and extreme loads are observed to have relatively complex trends with yaw offsets, which can change depending on the wind-speed regime. Good agreement is found between predicted and measured trends for both fatigue and ultimate loads.

1 Introduction

Despite numerous studies on the skewed inflow and wake of wind turbines (e.g., Hand et al., 2001; Schepers, 2004, 2012; Schreck and Schepers, 2014; Fleming et al., 2015), uncertainties still remain on the loading effects experienced by their mechanical components under misaligned operation. Whereas new interest is directed at maximizing plant power performance via wake steering and yaw control (e.g., Gebraad et al., 2016), understanding and managing their effects on operation and maintenance (O&M) costs is critical for the success of the strategy. For this reason, a clear understanding of the short- and long-term consequences of operating in skewed conditions, or with yaw offsets, is necessary to assess whether maintenance costs could change and to facilitate intelligent ways to improve power performance that mitigate any negative O&M impacts.

It can be argued that a certain degree of yaw error is always present during turbine operation, in part because of wind turbulence and in part because of mechanical errors in the turbine alignment and during yaw transients. Here we are concerned with the systematic, skewed-inflow operation. A few studies have shown a reduction in blade load levels for turbines operating under certain yaw offsets (e.g., Kragh and Hansen, 2014; Zalkind and Pao, 2016), accompanied by an increase in loads for other components (e.g., drivetrain and tower). Some focus has also been given to the load variations under cyclic variations of angle of attack (α) and relative air velocity at the airfoil of interest (U_{rel}), but conflicting information still exists. On the one hand, industry experts have either advised against yaw offset operation or devised technology and algorithms to minimize yaw

misalignment while maximizing power production at the individual turbines in a plant (Kragh and Hansen, 2015; Mortimer, 2016; Fleming et al., 2014). On the other hand, control system scholars recommend adopting strategies that can redirect wakes away from downwind turbines to increase the plant power production as a whole (e.g., Dahlberg and Medici, 2003; Wagenaar et al., 2012; Jiménez et al., 2010; Gebraad et al., 2016). In the middle, the owners and operators are left with the unsatisfying

5 conundrum of increasing power production and associated revenues while taking the risk of accelerated machine damage and associated repair costs.

Data from wind tunnel experiments (e.g., Schepers et al., 2011; Schreck and Schepers, 2014) show load and performance trends under yawed conditions, and emphasize the importance of dynamic stall and unsteady aerodynamics (UA) effects; yet these tests do not capture the impact of realistic atmospheric turbulence on the loads of key wind-power-plant components.

10 Some data from full-scale turbines are available (e.g., Boorsma, 2012), but are generally associated with involuntary yaw errors rather than a systematic measurement campaign with prescribed yaw offsets and comparison to aeroelastic simulations.

In this paper, we examine the problem of skewed wake and inflow for one utility-scale turbine configuration. The analysis starts from a theoretical standpoint and builds up in complexity, going from a simplified, analytical model for the α and U_{rel} azimuthal variations under different yaw offsets, to a fully aeroelastic realization of the turbulent operation. At one end of

15 the complexity spectrum, the analytical model is an aid to the designer, as it predicts load and performance outcomes under steady-state conditions and sheds light on the physics by highlighting the effects of shaft tilt, inflow shear, and yaw error. The aeroelastic model results, at the other end, account for turbulence effects and nonlinearities of the entire system and therefore provide more clarity about the system-dynamics response under realistic conditions. For practical predictions, the aeroelastic model should be validated, and extensive data were collected on a 1.5-MW turbine under several different yaw offset conditions

20 and compared to the model results.

In Section 2, we provide a description of the methods used in this study, the load channels of interest, and the turbine under analysis. In Section 3, the analytical model is presented. Section 4 provides results attained with simulations of the turbine operation under steady winds. Turbulent-inflow simulation results are compared to field-collected data in Section 5. A summary of the observations is offered in Section 6.

25 2 Methods and Load Channels of Interest

Our analysis was focused on the General Electric (GE) 1.5-MW SLE (GEWT) (Mendoza et al., 2015) installed at the National Wind Technology Center (NWTC), which is owned by the U.S. Department of Energy (DOE) and operated by the National Renewable Energy Laboratory (NREL). The turbine is instrumented with an extensive set of load and performance sensors per IEC (2015), which is described in the next section. An original GE aeroelastic model was modified to be used with NREL's

30 aero-hydro-servo-elastic tool for wind turbine design (FAST) version 8 (FASTv8) (Jonkman et al., 2015). FAST is a widely used industry and academic tool for loads estimation.

One of the underlying goals of this paper was to link the observed results to the physics of the blade aerodynamics and structural dynamics. Therefore, we started with a simplified model of the aerodynamics under steady, but sheared, wind con-

ditions and examined the azimuthal variation of the lift. An analytical model based on the variance of the lift out-of-plane component as a function of yaw offset was produced. The lift standard deviation, i.e., the square root of its variance, hence the associated blade load standard deviation, was used as an indicator of oscillating, fatigue loads. We then examined how this model performed under different hub-height wind speeds, and then increased complexity by first using AeroDyn 15,

5   FASTv8's aerodynamics module (AD15) in standalone mode, and then a fully aeroelastic model of the turbine within FASTv8. We demonstrated the effects of UA and of the structural response on the blade root bending moments by turning on and off FASTv8's UA module and the relevant structural degrees of freedom. This initial analysis was done based on two wind speeds, in turbine power regions 2 and 2.5. Finally, the model was further refined by accounting for turbulent inflow, and was compared to data from the field for several wind speeds up to rated power wind speed. Twenty turbulent seeds were considered, using

10 the IEC (2005) normal turbulence model (NTM), and the calculated loads were compared to those extracted from wind-speed binned data coming from the field. For the sake of brevity, results for only two wind speeds are shown, which, however, are representative of conditions at and below rated power.

Seven output channels of interest were selected: blade-root edgewise bending moment (EBM) and flapwise bending moment (FBM) and their resultant root-bending moment (RBM); low-speed-shaft torque (LSSTq); tower-top bending moment (TTBM)

15 (resultant of the fore-aft and side-side components); tower-top torque (TTTq); and tower-base bending moment (TBBM) (resultant of the fore-aft and side-side components). Initially, the focus is on the FBM because conflicting information exists in the literature and in the industry experience, and because it is also associated with thrust loads responsible for downstream component loading. The analysis was mainly carried out on fatigue loading, and the results are given in terms of short-term damage equivalent loads (DELs) via rainflow counting (Downing and Socie, 1982). Note that we also provide some insights on

20 ultimate loading, but they do not include parked and fault conditions. Simulations and field data are based on 10-min interval sets. In the next section, we describe the field instrumentation setup.

2.1   Field Instrumentation

The field-test campaign was carried out at the NWTC near Boulder, Colorado, and occurred over 6 months during which the test turbine was operated with discrete yaw offsets over a range of wind speeds and atmospheric conditions.

25   The test turbine and its dedicated meteorological tower are shown in Figure 1. Details of the turbine are provided in Table 1.

Table 1. Test Turbine Details.

Brand and Model	GE 1.5 SLE ESS
Parameter	Value
Rated Power (kW)	1500
Hub Height (m)	80
Nominal Rotor Diameter (m)	77
Rated Wind Speed (m/s)	14
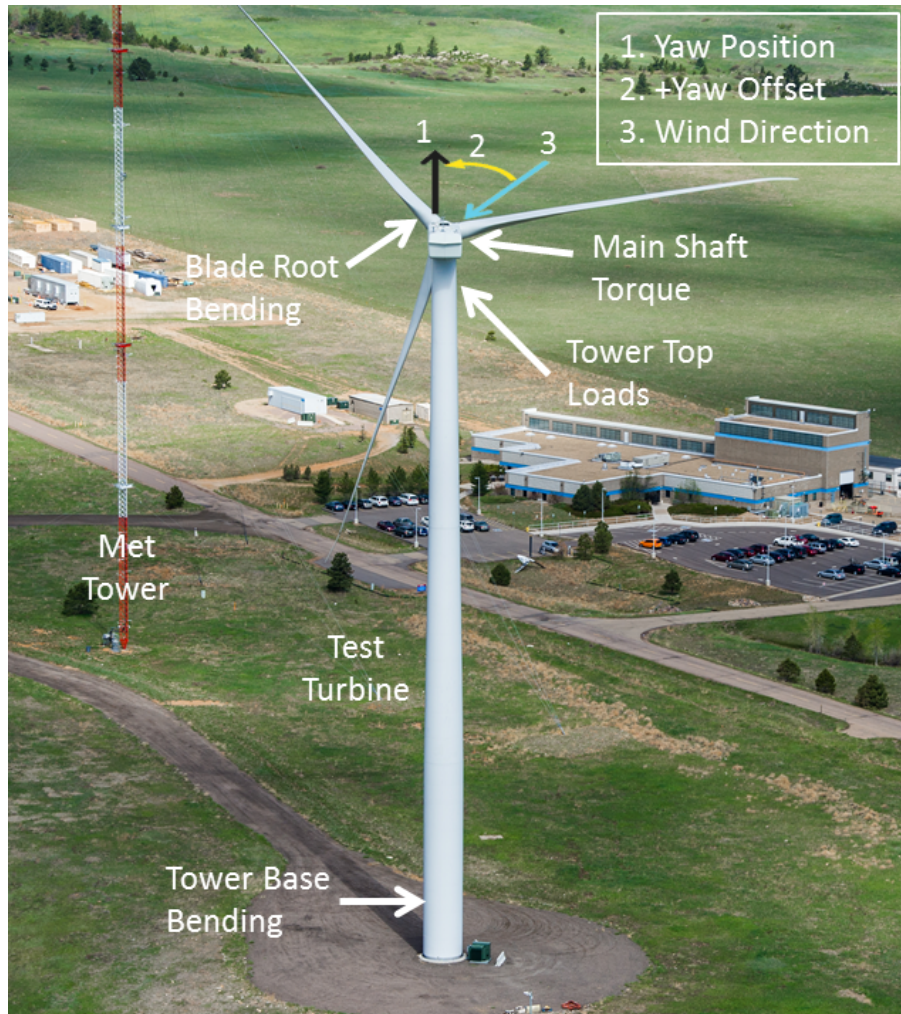
Figure 1. Test Turbine and Meteorological Tower, NREL 25911. Also shown is the adopted convention for positive yaw offset.

The turbine was instrumented in accordance with IEC 61400-13 (IEC, 2015) for mechanical loads measurements. All measurement methods and loads processing were in conformance with this standard. Specifically, the tower base, tower top, and blade roots were instrumented for measurement of bending loads. In addition, the tower top and main shaft were instrumented

5 for torque measurements. Encoders were used to measure yaw position, blade pitch, and rotor azimuth. The turbine was also instrumented for independent power measurements (per IEC, 2017). All signals were collected with a time-synchronous deterministic Ethercat protocol and stored at a sample rate of 50 Hz.

The meteorological tower is located 161 m (~2 rotor diameters) in the predominant upwind direction of the turbine and was instrumented in accordance with IEC 61400-12-1 (IEC, 2017). The meteorological tower measurement signals were time-synchronously recorded with the turbine loads signals. For the analysis presented in this paper, the 80-m cup anemometer and the 87-m wind vane signal were used for the reference mean wind speed, direction, and turbulence intensity. Test data was
5   limited to a sector of directions in which the meteorological tower is largely upwind of the turbine. This measurement sector avoids any turbine wake influence on the meteorological tower instrumentation or influence of other turbines at the test site. More details on the instrumentation set-up can be found in Dana et al. (2017-forthcoming).

The turbine nacelle's wind vane signal was modified using a frequency modulation device with a dedicated user interface for programming yaw offset schedules of discrete offset values and durations. In no other way was the turbine or its controller
10 manipulated. The turbine was set to cycle at 1-hr intervals between the baseline setting, i.e., a 0° yaw offset, and a nonzero offset. The offset values included -25°, -18°, -12.5°, 0°, 12.5°, 18.0°, and 25.0°. However, not all offset value data could be used for analysis because of wind speeds or directions outside of the acceptance ranges selected for this study and discussed below.

As visible in Figure 1, the convention employed for the sign of the yaw misalignment implies that with positive yaw offset
15 the hub center is to the right of the tower centerline when looking downwind.

3   Analytical Simplification

Fundamentally, the dominant loads during turbine operation originate from the aerodynamic forces and moments on the rotor blades. The largest contributor to the design loads on the blades and the downstream components is the lift distribution acting on the blade airfoils. Examining how the out-of-plane (rotor axial) component of the lift varies as a function of azimuth under
20 different yaw angles can help explain the cyclic out-of-plane loading at the blade root and therefore the associated variation of several component loads (e.g., tower, drivetrain). The axial component ($\hat{l}$) of the two-dimensional (2-D) airfoil lift can be written as:

$$\hat{l} = \frac{1}{2}\rho_a U_{rel}{}^2 c_l(\alpha) c \cos\phi \tag{1}$$

where ρ_a is the air density, c is the chord, $c_l(\alpha)$ is the 2D lift coefficient, α is the angle of attack, ϕ is the inflow angle, and
25 where effects on c_l due to airfoil-chord Reynolds Number and Mach number are ignored. At a first approximation, within the linear region of the airfoil lift polar, one could assume:

$$c_l(\alpha) \simeq c_1 \alpha \tag{2}$$

where c_1 is an airfoil constant ($\simeq 2\pi$ for thin airfoils). As we are interested in fatigue loads, the standard deviation of $\hat{l}$ can be used as a surrogate for the load oscillation significance. Besides a constant, this translates to the standard deviation of
30 the product between $c_l \cos\phi (\simeq c_1 \alpha \cos\phi)$ and U_{rel}^2. To this end, through basic trigonometry, α and U_{rel} can be written as in

Eqs. (3)-(4):

$$\alpha\left(\psi, r, \theta, U_{hub}, \omega, \gamma\right) = \phi - \theta = \arctan \frac{U(\psi, r, U_{hub})\cos(\gamma)\cos(\delta)}{v_t(\omega, r) - U(\psi, r, U_{hub})\left[\cos(\gamma)\sin(\delta)\sin(\psi) + \sin(\gamma)\cos(\psi)\right]} - \theta \tag{3}$$

$$U_{rel}\left(\psi, r, U_{hub}, \omega, \gamma\right) = \sqrt{\left[U(\psi, r, U_{hub})\cos(\gamma)\cos(\delta)\right]^2 + \left[v_t(\omega, r) - U(\psi, r, U_{hub})\left[\cos(\gamma)\sin(\delta)\sin(\psi) + \sin(\gamma)\cos(\psi)\right]\right]^2} \tag{4}$$

5   where ψ is the rotor azimuth angle, r is the blade station radial position, θ is the airfoil aero-twist plus pitch setting, δ is the shaft tilt, ω is the rotor rotational speed, γ is the rotor yaw offset, $v_t(\omega, r)$ is the airfoil tangential (in-plane) velocity, and $U(\psi, r, U_{hub})$ is the wind speed at the elevation identified by ψ and r station, and function of the U_{hub}, where U_{hub} is the hub-height mean wind speed. Note that a power-law shear is included in $U(\psi, r, U_{hub})$. Under the hypothesis of constant and uniform induction in region 2 of the turbine power-production curve, we ignore induction and tip effects that would translate

10   in a constant bias in α and c_l for most of the power-producing blade span.

In Figure 2, α and U_{rel} calculated by this analytical model are plotted as a function of ψ for the 75% blade span station under various yaw offsets and for U_{hub}=12 m/s with a power-law shear exponent value of 0.2[1]. It can be seen that the impact of yaw offset reflects primarily on increasing the amplitude of the oscillations for both α and U_{rel}, with little change in the mean values. Of special note are the azimuthal loci of maxima and minima of the two quantities, which are shifted away from ψ=0° and 180°, demonstrating an asymmetry in the distribution of lift between the left and right halves of the rotor plane.
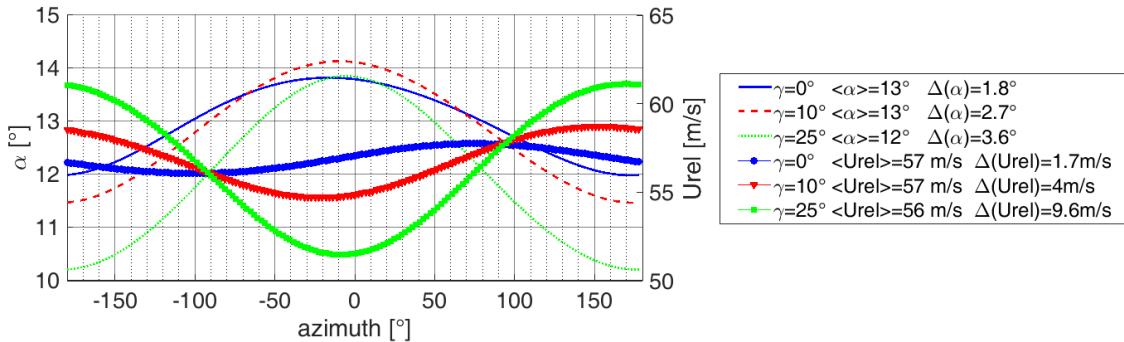
Figure 2. α (lines with no markers) and U_{rel} (lines with markers) calculated by the simplified analytical model as a function of ψ for the 75% blade span station under yaw misalignments (γ) as shown in the legend; U_{hub}=12 m/s. In the legend, the $<>$ and Δ denote mean and range (max-min) of the argument.

---

[1]The sign convention adopted for the yaw offset is shown in Figure 1.

As shown by Eqs. (3)-(4) and Figure 2, α and U_{rel} are two quantities well correlated, thus we can use basic statistics (e.g., Frishman, 1975) to find the covariance of the product $c_l \cos\phi U_{rel}^2$ as in Eq. (5):

$$\sigma^2\left(c_l \cos\phi \cdot U_{rel}^2\right) \simeq \sigma^2\left(\alpha \cos\phi \cdot U_{rel}^2\right) = \sigma^2_{\alpha\cos\phi \cdot U_{rel}^2} =$$

$$\sigma^2_{(\alpha\cos\phi)^2, U_{rel}^4} + \left[\sigma^2_{\alpha\cos\phi} + \overline{\alpha\cos\phi}^2\right] \cdot \left[\sigma^2_{U_{rel}^2} + \overline{U_{rel}^2}^2\right] - \left[\sigma^2_{\alpha\cos\phi, U_{rel}^2} + \overline{\alpha\cos\phi}\,\overline{U_{rel}^2}\right]^2 \qquad (5)$$

In Eq. (5), σ^2 denotes the covariance or variance of the argument, and overbars indicate the means of the variables; furthermore,

5 the constant c_1 is omitted with no loss of generality.

In Figure 3, the model calculated standard deviations for the 75% span airfoil's $c_l \cos\phi$, U_{rel}^2, and their product are shown for different values of yaw offsets and hub-height wind speeds of 8 and 14 m/s with a wind shear exponent of 0.2. The standard deviations were normalized by the means of their respective variables, and are indicated as $\hat\sigma_{c_l\cos\phi}$, $\hat\sigma_{U_{rel}^2}$, and $\hat\sigma_{c_l\cos\phi \cdot U_{rel}^2}$, respectively. The rotor rotational velocity was set at the average value obtained from aeroelastic simulations and verified against actual turbine field data for that wind speed. The graphs show that whereas $\hat\sigma_{U_{rel}^2}$ displays a minimum at 0° yaw,
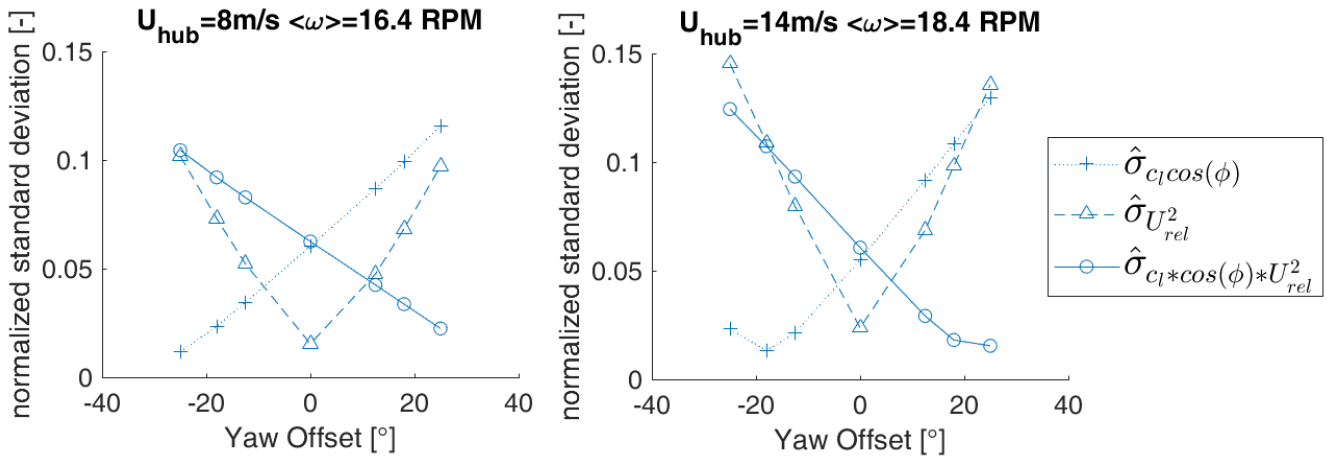
Figure 3. Standard deviations of $c_l \cos\phi$ (crosses), U_{rel}^2 (triangles), and their product (circles) for the airfoil at $\sim 75\%$ of the blade span, for two U_{hub} wind speeds of 8 m/s (left) and 14 m/s (right), wind shear exponent value of 0.2, and mean rotor rotational speed of ω=16.4 (left) and 18 rpm (right). The standard deviations are normalized by the means of the respective arguments.

the $\hat\sigma_{c_l\cos\phi}$ has a minimum near $-20°$. By examining other wind-speed cases (not shown), which in general rendered similar trends to Figure 3, it was observed that the minima in $\hat\sigma_{c_l\cos\phi}$ and $\hat\sigma_{c_l\cos\phi \cdot U_{rel}^2}$ get closer to the γ=0° location with increasing wind speed. Both the $\hat\sigma_{c_l\cos\phi}$ and $\hat\sigma_{U_{rel}^2}$ curves in Figure 3 show an asymmetric behavior. The $\hat\sigma_{U_{rel}^2}$ standard deviation, for example, shows higher values for negative yaw offsets than for the corresponding positive misalignments. In contrast, $\hat\sigma_{c_l\cos\phi}$

15 exhibits larger variations for positive yaw offsets. The $\hat\sigma_{c_l\cos\phi \cdot U_{rel}^2}$ standard deviation, however, decreases sharply going from negative to positive misalignments, with a reduction of some 66% at γ=25° with respect to the baseline case of γ=0°. This

simplified analysis suggests that, at least in terms of aerodynamic load oscillations, positive yaw misalignments could lead to a considerable load range reduction. Similar trends were observed at other span locations (not shown).

Although this analysis only considered steady winds, rigid blades, steady aerodynamics, and no induction, it brought forth results in agreement with recent studies. Zalkind and Pao (2016), for example, suggest the existence of an asymmetric behavior

5   of blade and tower fatigue loads hinting at the same positive offset as load-favorable misalignment direction.

4   Blade Aerodynamics and Structural Dynamics under Steady Winds

To better assess the physics responsible for fatigue loading under skewed inflow conditions, and to verify the existence of a preferred misalignment direction for loads, we build up models of increasing complexity utilizing AD15 and the full FASTv8 aeroelastic tool under steady winds.

10   Figure 4 shows azimuthal trends for α and U_{rel} as calculated by AD15 for the 75%-span station with aligned, sheared flow (0.2 power-law exponent) and no induction effects. It can be observed that α achieves a maximum before reaching the azimuthal zenith, and a minimum affected by the tower shadow effects just before the 180° azimuth; U_{rel} exhibits an analogous trend, though shifted by 180°. The asymmetry is caused by the combination of the nonlinear wind profile (power-law) and the trigonometric contribution of the airfoils' rotational speed to the relative air speed as a function of their positions

15   (advancing/retreating effect). Therefore, the sole presence of shear and tilt causes an asymmetry in the variation of $c_l(\alpha)$ and U_{rel} even under no yaw offset conditions, which can affect the performance of both the individual machine and the entire plant. For example, it can be speculated that under significant shear, the optimum power performance could occur under misaligned conditions. Furthermore, the asymmetric distribution of α and U_{rel} translates into an asymmetric azimuthal distribution of the induction factors, which in turn offsets the wake axis. A power increase under yaw offset conditions is suggested by Kragh and

20   Hansen (2014), and reports of skewed wake under aligned inflow conditions have been presented in Annoni et al. (2016) and Vollmer et al. (2016). These aspects are not further analyzed in this study, however.

By adding yaw offset, the asymmetry about the 0–180° azimuth is still present (see also Figure 2), and whereas the azimuthal mean α values slightly decrease with larger yaw offsets, the α-ranges (max-min, denoted by 'Δ') increase with increasing offsets. Table 2 shows the range for α, c_l, and U_{rel}^2 at different blade spanwise stations (given as spanwise fractions, b_f =0.28–

25   0.92) for two hub-height wind speeds (8 and 12 m/s) and for γ=0°, -10°, and 10°. From the table, it can be observed that, relative to the aligned cases, α-ranges reduce by 16–30% with negative misalignments, and increase by 14–70% with positive ones. This is in agreement with the analytical model predictions. Also, when compared to the aligned cases, the c_l-ranges tend to be larger (smaller) for positive (negative) offsets. The U_{rel}^2-ranges, however, increase for both directions of misalignment, but increase more under negative offsets. As these effects oppose each other when generating aerodynamic loads, it is difficult

30   to ascertain whether one offset direction could lead to a more favorable load response. Furthermore, as shown in Table 2, the reduced frequencies ($k = \dfrac{d\alpha}{dt} c / (2U_{rel})$, where c is the chord length and t denotes time) associated with the azimuthal α variations are largely above 0.02, which is the commonly accepted threshold for unsteady aerodynamic effects to take place
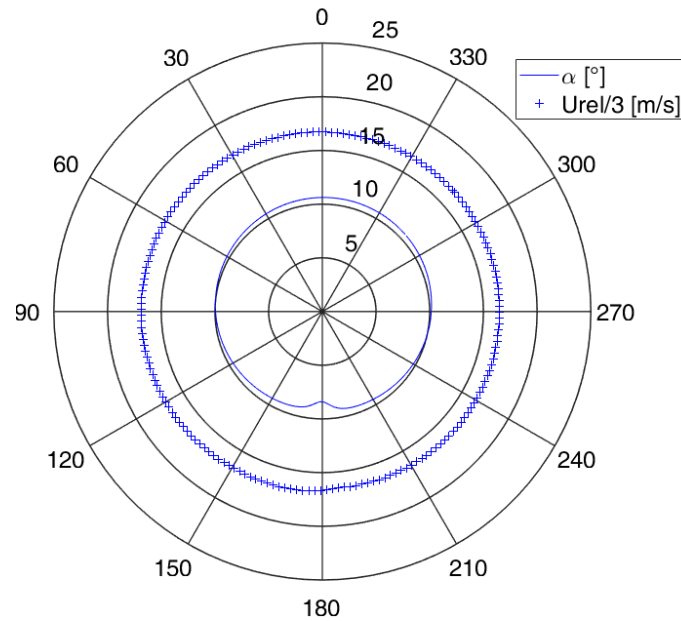
Figure 4. α and U_{rel} (magnitude divided by three) for the 75% span airfoil as a function of ψ under aligned conditions and a steady hub-height wind speed of 8 m/s as calculated by AD15. The view is from downwind of the rotor.

(Damiani et al., 2016). Given the expected higher values in angles of attack under positive yaw offsets, dynamic stall effects should be more prevalent with those misalignments.

Table 3 offers similar results as Table 2, but with induction, skewed wake correction (Ning et al., 2015), and UA effects included. For most blade spans and wind speeds, AD15 returned increased ranges of α with respect to the no-induction, geometric calculations. Overall, however, the trends explored under no-induction still apply, with positive yaw offsets showing larger variations in c_l but smaller in U_{rel}^2, confirming that the assumptions in the analytical model of constant and uniform induction are reasonable. By enabling UA (Damiani et al., 2016), higher peaks in c_l's especially inboard of the blade were noted. As visible in Figure 5, which portrays azimuthal traces for c_l at four blade spanwise stations with no UA (Figure 5a) and with UA (Figure 5b) effects, the impact of UA is mostly associated with a sharp stall transition for the inboard airfoils (at rotor radius $\leq 30\%$), which is discussed below.

Figure 6a shows the basic statistics of the blade-root FBM and EBM as calculated by a complete FASTv8 model of the turbine under investigation for yaw offsets ranging from $-25°$ to $25°$ and for 8- and 12-m/s hub-height wind speeds. The companion Figures 6b and 6c offer similar results as obtained by excluding either UA or the rotor/tower flexibility, respectively. In the plots, the 25th and 75th percentiles of the loads' distributions are marked with the left and right sides of rectangular boxes, respectively; the line in the middle of each box is the median, and the whisker lines show the distances to the most extreme sample values within the 1.5 interquartile range (i.e., 1.5 times the width of the box). Data beyond 1.5 times the interquartile ranges are shown as outliers with red crosses. Figure 6a shows little variation of the EBM statistics as a function

Table 2. Ranges (Δ) for α, c_l, and U_{rel}^2 as calculated by AD15 (without induction) for various blade stations (b_f) and hub-height wind speeds (U_{hub}) and for yaw offsets (γ) of $0°$, $-10°$, and $10°$. A wind shear exponent of 0.2 was assumed. The calculated reduced frequencies (k) for the various airfoil stations are also given.

U_{hub}	b_f	$\gamma=0°$				$\gamma=-10°$ [a]			$\gamma=10°$ [a]		
		$\Delta(\alpha)$	k	$\Delta(c_l)$	$\Delta(U_{rel}^2)$	$\Delta^*(\alpha)$	$\Delta^*(c_l)$	$\Delta^*(U_{rel}^2)$	$\Delta^*(\alpha)$	$\Delta^*(c_l)$	$\Delta^*(U_{rel}^2)$
[m/s]	[-]	[°]	[-]	[-]	[m²/s²]	[-]	[-]	[-]	[-]	[-]	[-]
	0.28	4.4	0.11	0.38	63	-0.16	-0.05	1.47	0.57	0.00	1.07
8	0.51	2.9	0.046	0.11	91	-0.31	-0.19	1.85	0.31	0.45	1.46
	0.76	2.2	0.02	0.09	120	-0.18	-0.15	1.92	0.23	0.24	1.58
	0.92	2.1	0.011	0.09	132	-0.19	-0.14	2.18	0.14	0.17	1.73
	0.28	5.7	0.11	0.03	115	-0.14	0.07	1.39	0.70	0.30	0.87
12	0.51	3.7	0.045	0.06	168	-0.32	-0.63	1.62	0.46	1.68	1.14
	0.76	3	0.02	0.07	217	-0.30	-0.10	1.84	0.27	0.01	1.37
	0.92	2.7	0.011	0.07	245	-0.22	-0.01	1.94	0.22	0.01	1.44

[a] Δ^* denotes the relative difference in range of the argument, with respect to the same quantity at 0° yaw offset.

(a) without UA   (b) with UA
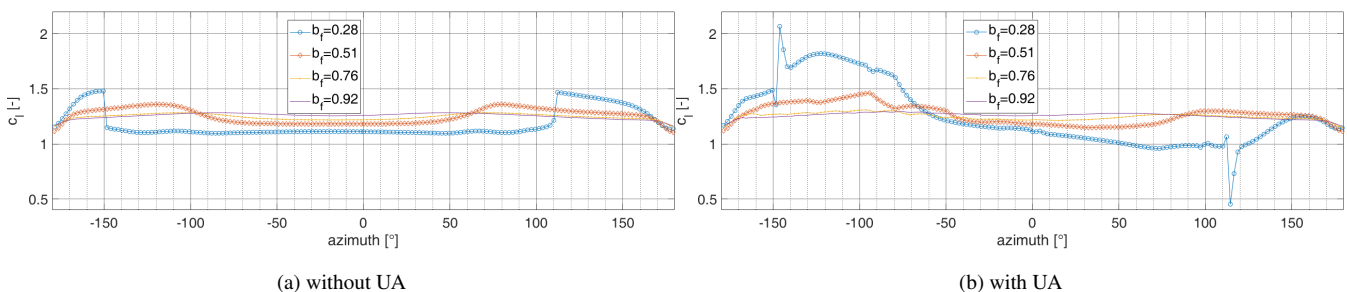
Figure 5. (a) c_l vs. ψ for various blade stations (b_f) and for $\gamma=10°$ offset as calculated by AD15 for a hub-height wind speed of 12 m/s. (b) as in (a) but with UA effects included.

of yaw offset and wind speed; this outcome is to be expected, as the EBM is mainly driven by gravity loads. The FBM median is seen to decrease with nonzero yaw offsets, as one would expect as the mean thrust load reduces. The FBM distribution interquartile, hence the variance and standard deviation, however, get larger with nonzero offsets, and more pronouncedly so for negative yaw offsets. Note that, in contrast to this result, the analytical model of Section 3 predicted an increase in variance

5   for negative yaw offsets, but a decrease for positive misalignments.

Data associated with Figure 6 results demonstrate that the standard deviations tend to increase (except at the highest yaw offset) when UA is excluded from the computations. This indicates that UA acts as a low-pass filter on the span-integral load.

Table 3. Ranges (Δ) for α, c_l, and U_{rel}^2 as calculated by AD15 (with induction) for various blade stations (b_f) and hub-height wind speeds (U_{hub}) and for yaw offsets (γ) of 0°, −10°, and 10°. A wind shear exponent of 0.2 was assumed. Results for $\Delta(c_l)$ are given with (UA) and without (nUA) unsteady aerodynamics effects included.

U_{hub}	b_f	γ=0°				γ=−10° [a]				γ=10° [a]			
		$\Delta(\alpha)$	$\Delta(c_l)$		$\Delta(U_{rel}^2)$	$\Delta^*(\alpha)$	$\Delta^*(c_l)$		$\Delta^*(U_{rel}^2)$	$\Delta^*(\alpha)$	$\Delta^*(c_l)$		$\Delta^*(U_{rel}^2)$
[m/s]	[-]	[°]	nUA [-]	UA [-]	[m²/s²]	[-]	nUA [-]	UA [-]	[-]	[-]	nUA[-]	UA[-]	[-]
8	0.28	3.2	0.37	0.31	63	-0.16	-0.16	-0.26	1.47	0.63	0.59	0.65	1.07
	0.51	2.6	0.3	0.27	91	-0.31	-0.30	-0.37	1.69	0.38	0.40	0.44	1.38
	0.76	2.6	0.26	0.24	120	-0.19	-0.35	-0.21	1.92	0.27	0.23	0.25	1.58
	0.92	2.1	0.2	0.19	132	-0.14	-1.00	-0.11	2.18	0.24	0.20	0.26	1.73
12	0.28	8.9	0.38	1.7	115	-0.07	0.00	0.00	1.39	0.46	0.00	0.12	0.87
	0.51	4.9	0.17	0.25	168	-0.37	-0.35	0.04	1.62	0.39	0.47	0.40	1.14
	0.76	3.5	0.089	0.12	217	-0.34	-0.16	0.00	1.84	0.29	0.46	0.33	1.37
	0.92	2.9	0.093	0.1	245	-0.24	-0.09	-0.10	1.94	0.24	0.29	0.30	1.44

[a] Δ^* denotes the relative difference in range of the argument, with respect to the same quantity at 0° yaw offset.

Furthermore, under rigid conditions, the FBM values are generally associated with slightly lower standard deviations, whereby it can be expected they would lead to lesser fatigue loads. These observations are confirmed by an analysis of the load variation as a function of azimuth (not shown for the sake of brevity), which translate into smoother curves.

In Figure 7, the calculated short-term FBM DELs are presented for U_{hub}=8 and 12 m/s, and for three different configurations: one including the entire model physics, one without UA effects, and one without blade (and tower) flexibility. The complete model results show a minimum of the DEL for the aligned conditions, although the asymmetry in the loading persists, with negative yaw offsets rendering larger loads than the positive counterparts. The second set of results in Figure 7 is only slightly different from the first and thus confirms that the dynamic stall effects are not so important for the trends observed in blade root loads, despite showing a noticeable effect on the c_l's as shown in Figure 5. This result suggests that the integral of the lift distribution along the blade span washes out the UA contribution to the oscillating loads. Finally, with rigid blades and U_{hub}=8 m/s, the trend for the root FBM DEL is as expected from the simplified variance model of Section 3. Therefore, at this wind speed, the inertial forces associated with the elastic response—of the rotor in particular—have a dominant effect on the calculated DELs.

At U_{hub}=12 m/s, however, the DEL trend with yaw offset reflects what is observed in the first set of Figure 7, suggesting that the load variation with yaw offset at this wind speed is only slightly affected by the structural response, and therefore

(a) Complete Model (b) No UA (c) Rigid Blades
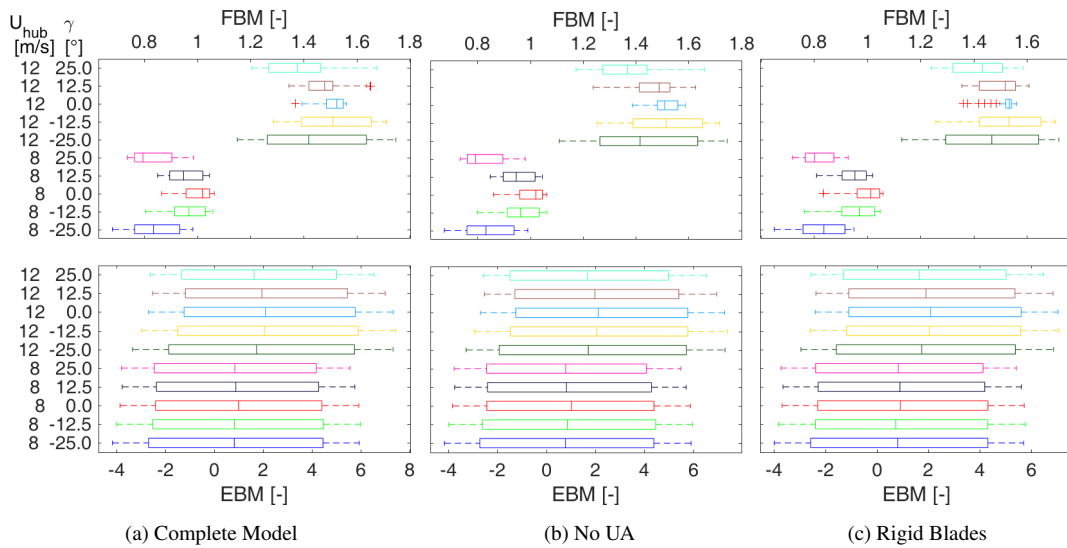
Figure 6. (a) Nondimensional FBM (top) and EBM (bottom) boxplot statistics for the various cases of U_{hub} (8 and 12 m/s) and γ (−25° to 25°) as indicated along the y-axis, as calculated by FASTv8 for a complete model of the GEWT. The loads are normalized by the respective means at 8 m/s and 0° yaw offset; (b) as in (a) but calculated excluding UA effects and (c) as in (a) but calculated with rigid blades and tower.
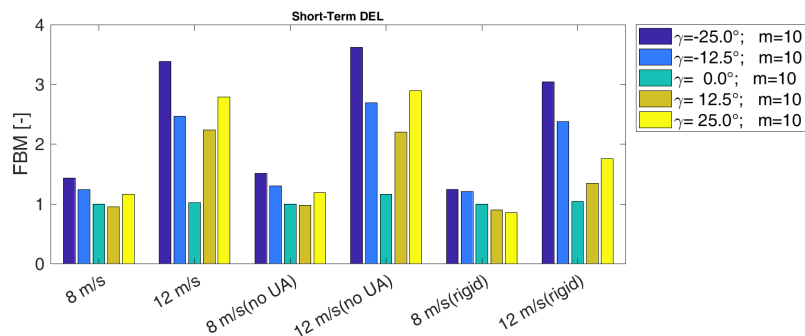
Figure 7. Blade-root FBM short-term DEL with yaw offsets from −25° to 25° as calculated by FASTv8 for U_{hub}=8 and 12 m/s. Also shown are results obtained either by excluding UA (denoted by 'no UA') or by removing structural rotor flexibility (denoted as 'rigid').

primarily driven by pure aerodynamic loading[2]. To understand what is happening at 12 m/s, we further examined the blade c_l-vs.-azimuth relationship. Figure 8 shows how blade structural flexibility affects the c_l-vs.-azimuth trends for various blade span stations at γ=12.5° and for U_{hub}=8 and 12 m/s. At the higher wind speeds, the inboard airfoils start stalling, even at γ=0°, and the abrupt drop in c_l creates a load forcing that contributes to the higher DELs. This can also be observed in Figure 5.

5   By comparing Figure 8a to Figure 8b, one can note the 100% increase in the c_l-range for the station near the 30% blade span when going from U_{hub}=8 m/s to U_{hub}=12 m/s. Furthermore, by comparing Figures 8a–8b to Figures 8c–8d, one can see that, at U_{hub}=12 m/s, the lift curves are almost unchanged when the blades are made rigid, as opposed to the case with 8-m/s hub-height wind speed, where the blade flexibility returns a more complex c_l response in the region of tower influence near the 180° azimuth for the outboard airfoils, thus again leading to expected higher fatigue loading. This analysis explains why, at the

10   higher wind speeds, the impact of flexibility is almost negligible on the FBM short-term DEL trend with yaw misalignment, but how suppressing elastic response at the lower wind speeds can significantly change the fatigue loading level.
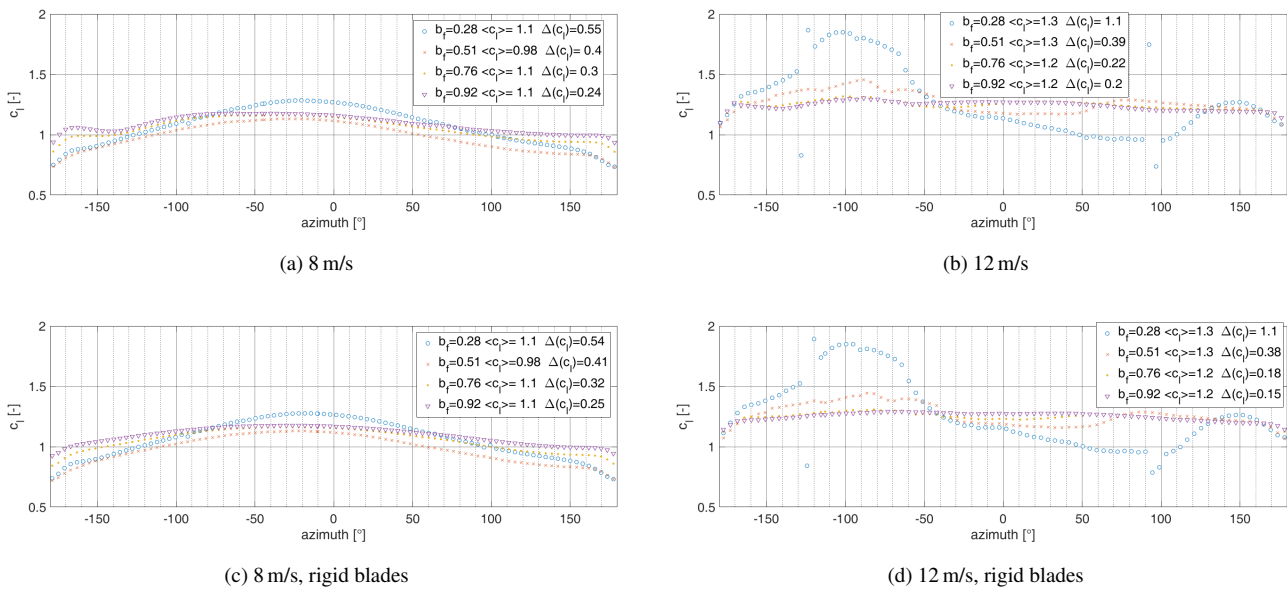
Figure 8. FASTv8 results with steady winds; (a) c_l vs. ψ for 8 m/s wind speed and 12.5° yaw offset, (b) as in (a) for a hub-height wind speed of 12 m/s, and (c) and (d) as in (a) and (b) but with rigid blades and tower. Note that the legends provide mean (denoted by <>) and range (max-min) of c_l for the various span stations (b_f).

Figure 9 further demonstrates how the blade inboard stations exhibit a sharp drop in lift near stall. The combination of higher α's with higher wind speeds, and the sharper airfoil stall characteristics of the inboard airfoils, cause the large variations in c_l's, which in turn are responsible for the increase in oscillating loads at the root. This nonlinear aerodynamics explains why the

15   simple variance model cannot capture load trends at higher wind speeds, and therefore indicates that the airfoil characteristics

---

[2]Note that the turbine controller constantly varies the pitch of the blades at this speed and at all the yaw errors examined thus far, but it was verified that disabling the controller in the simulations does not significantly affect these observations.
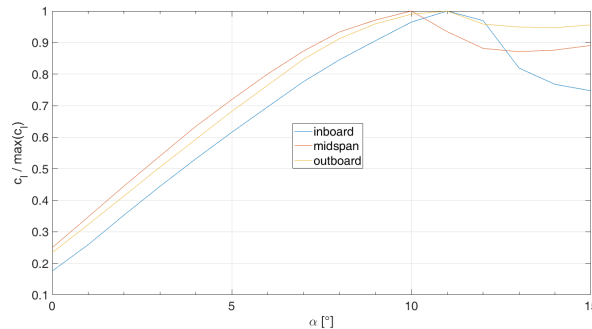
Figure 9. Lift polar curve of the inboard to midspan airfoils normalized to the respective maximum c_l's.

and the associated UA, together with the elastic response of the blades, contribute to the actual fatigue loading of the blade, and thereby all the downstream turbine components. Given these results, one can only rely on accurate, nonlinear, aeroelastic models of the turbine and thorough loads analyses to assess the loading levels in the various components under yaw offsets. In the subsequent section, we carry out a loads analysis based on FASTv8 simulations with turbulent winds, and compare the

5   predictions to field-measured loads.

5   Aeroelastic Simulation and Field Data Validation

To compare model predictions to actual field measurements, we ran aeroelastic simulations for hub-height mean wind speeds ranging from 4 to 24 m/s in 2-m/s wind-speed bins, and with NTM inflow (see also IEC, 2005) with 20 turbulence seeds per wind-speed bin. However, besides brevity, we limit the discussion to mean hub-height wind speeds of 10 and 14 m/s for three

10   reasons. First, we intend to compare to data bins from the field, thus we selected those that provided sufficient field data points for statistical significance. Second, above rated wind speed, pitch dynamics adds more complexity to the interpretation of the results. Lastly, low wind speeds ($\leq$ 6 m/s) gave rise to shutdowns in the simulations, which we wanted to exclude for the sake of clarity. Furthermore, the selected wind speeds are representative of conditions at or below rated power, which is where wake steering is thought to be most effective.

15   The investigated yaw offsets ranged from $-25°$ to $25°$, which have been considered for wake redirection in wind farms. Because the field data showed large variations in turbulence intensity (TI) within individual wind-speed bins (see Figure 10), a lower turbulence range was selected for the simulations, with a mean TI=15% throughout the wind-speed range. Accordingly, the field data were filtered to retain measurements with TI ranging from 1 to 17% to guarantee a statistically significant number of samples. This was necessary because turbulence intensity proved to have a larger effect than the sole yaw offset on the

20   magnitude of DELs, as can be seen, for example, in the blade-root FBM DELs shown in Figure 11.
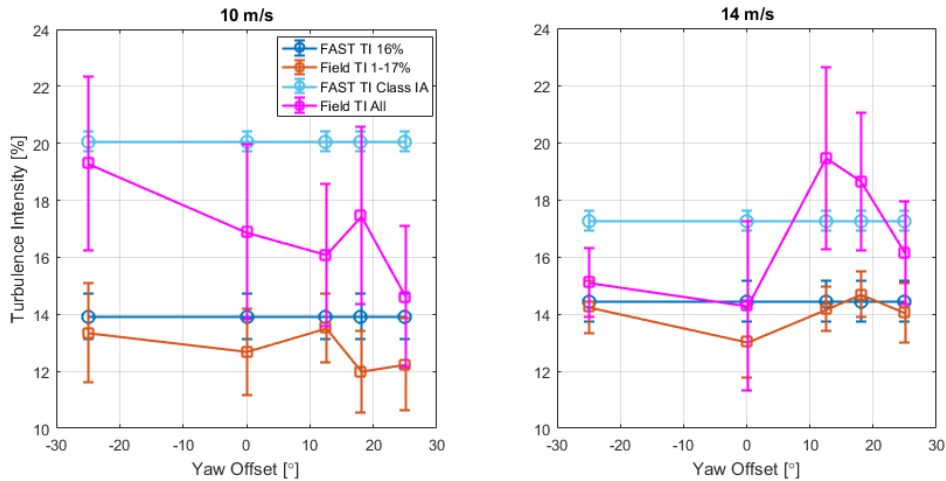
Figure 10. Comparison between simulated (circles) and measured (squares) values of TI as function of yaw offset for two wind-speed bins of interest (left: U_{hub}=10 m/s; right: U_{hub}=14 m/s). The field data are shown when including all data (label "All" in the legend) and when filtering for TI below 17% (label "TI 1–17%" in the legend). The simulated data are shown for Class IA turbulence (IEC, 2005) (label "FAST TI Class IA" in the legend) and for TI=16% at 15 m/s (label "FAST TI 16%").
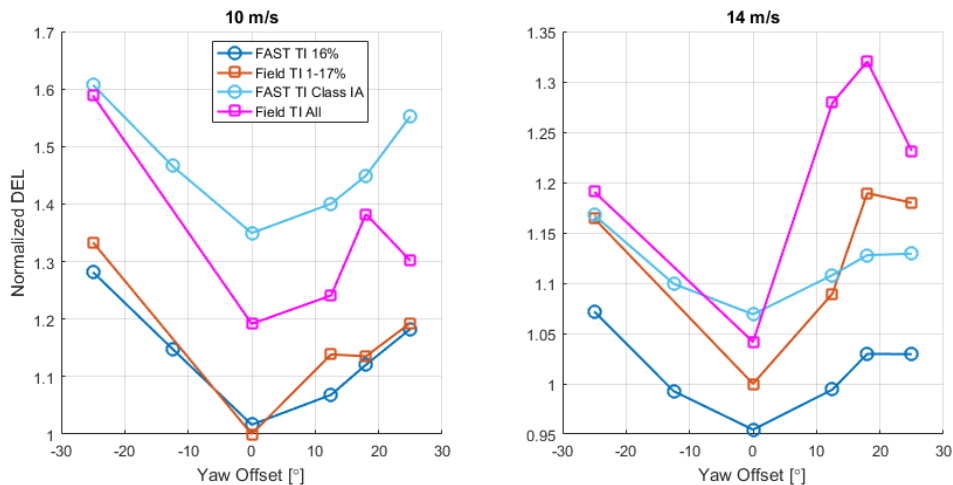
Figure 11. TI effect on the blade FBM DEL. Comparison between simulated (circles) and measured (squares) values of the loads for various TI levels, as a function of yaw offset and for U_{hub}=10 m/s (left) and U_{hub}=14 m/s (right). The loads are normalized by the mean value at 0° yaw offset from the field data filtered to a TI range of 1 to 17%. Labels in the legend are the same as in Figure 10.

5.1 Fatigue Loads

Figure 12 offers a summary comparison between predicted and measured short-term DELs for the various channels of interest and for 10 and 14 m/s. The bars represent mean values from simulation results, and the square symbols are the corresponding values derived from the field measurements. For each channel, the mean values are given as a function of yaw offset, with all

5   DELs normalized by the field value at the zero yaw offset. Because field data at $\gamma=-12.5°$ were scarce, they were not included in the plots. In Appendix A, Figures A1–A7 show detailed comparisons between the predicted and the measured DELs for the various load channels of interest as a function of yaw offset and including error bars representing ± 1 standard deviations. The spread comes from multiple seeds in the FAST results, and from multiple data points (10-min records) in the field datasets.
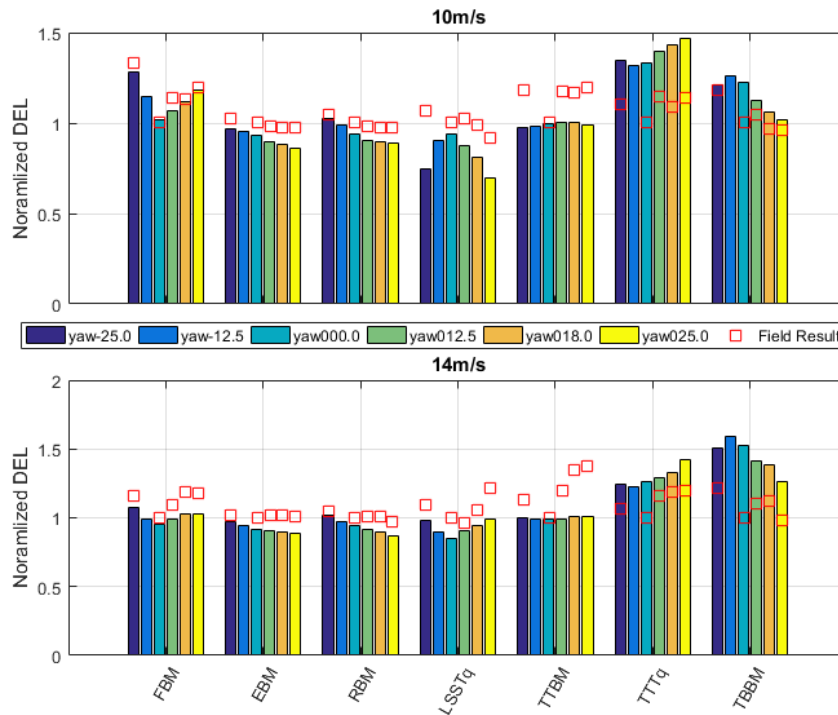
Figure 12. Comparison between predicted (FAST, bars) and measured (field, square symbols) mean DELs as a function of yaw offsets, for mean $U_{hub}=10$ m/s (top) and 14 m/s (bottom). DELs are normalized by their respective mean measured values at 0° yaw offset and $U_{hub}=14$ m/s.

Overall, good agreement was observed between predicted and measured data both in absolute terms and as far as yaw-offset

10   trends are concerned. For example, the FBM values predicted at the blade root are very close to the corresponding field-derived data. A minimum is seen under aligned conditions as was also shown under steady-state wind conditions in Section 4. The

previously observed asymmetry in the mean loading as a function of yaw offset is still visible, with negative yaw errors giving rise to larger loads, though at 14 m/s, this effect is not confirmed by the field-derived data.

Both the calculated and measured blade-root EBM display a mostly monotonic, decreasing trend with increasing yaw offset, although less pronounced at 14 m/s. This decreasing trend is in line with the decrease in standard deviations observed in Figure 6a under steady conditions, and is attributable to the aerodynamics partially relieving the gravity loading when going from negative to positive yaw offsets.

To assess the effective fatigue load on the blade root, the resultant unsymmetric RBM must be analyzed via *load roses*, wherein multiple circular sectors of the root cross section are considered, in addition to the 0° (FBM) and 90° (EBM) components. Eight sectors, each 22.5° wide, were analyzed, and the data from the largest contributing sector from each yaw offset were selected and normalized with respect to the field value under aligned conditions. The calculated results demonstrate that the resulting fatigue loading decreases with increasing yaw offset, and that negative misalignments appear more detrimental than the aligned conditions. The field-derived results generally confirm this trend, but not as clearly.

The LSSTq DELs also showed good agreement between predicted and measured data, especially at 14 m/s. Note, however, the reversal in the trend with yaw misalignments for different wind speeds. For wind speeds below 14 m/s and near $\gamma=0°$, in fact, FAST results exhibited a maximum in torque DEL, whereas they showed a minimum for a wind speed of 14 m/s. The field-derived data confirm this reversal, although an outlier can be noted at $\gamma=-25°$ and 10 m/s.

A more significant discrepancy was observed for the mean resultant TTBM DEL. The load-rose analysis of field data (conducted in the same fashion as for the blade-root loads above) exhibits an increase in the short-term fatigue damage for nonzero yaw offsets. FAST predictions, however, render a much smaller effect of the yaw misalignment. The largest discrepancy between field and FAST results (~40% relative error) can be seen at $\gamma=25°$ and 14 m/s, but it is also accompanied by very large standard deviations in the field data (see Figure A5).

The TTTq DEL from measurements at tower top is, on average, overestimated by the simulations. Large variations in the loading levels, however, can be seen for positive yaw offsets and higher wind speeds both in the field data and in the predictions (see Figure A6). Notwithstanding this discrepancy (up to 17% relative error), the increase in torque with increasing yaw misalignment is confirmed by both simulation- and field-derived data.

At the tower base, FAST predicts that the resultant TBBM DELs (calculated through load roses) have a maximum between 0° and −12.5° yaw offsets. Measurements from the field, however, lead to a significant increase of the DELs with negative yaw offset (−25°), and a somewhat lesser increase for positive yaw offsets except at the higher wind speeds. The field-derived data at −25° still appear to be outliers. The largest relative error in the calculated DEL was 50% under aligned conditions and 14 m/s.

5.2 Extreme Loads

To complete this gallery of results, we offer a comparison between the FAST-predicted extreme loads and those measured in the field. Note that these loads are not necessarily the highest loads the various components would encounter throughout the turbine lifetime, but they give an idea of what to expect in a relative sense when the turbine is operated under misaligned

conditions. Similarly to what was done for the DELs, a summary graph for the mean load values is given in Figure 13 for all the main channels of interest. The extreme loads were normalized by the mean recorded in the field at 14-m/s wind speed and 0° yaw. Detailed trends and graphs for individual load channels are given in Dana et al. (2017-forthcoming).
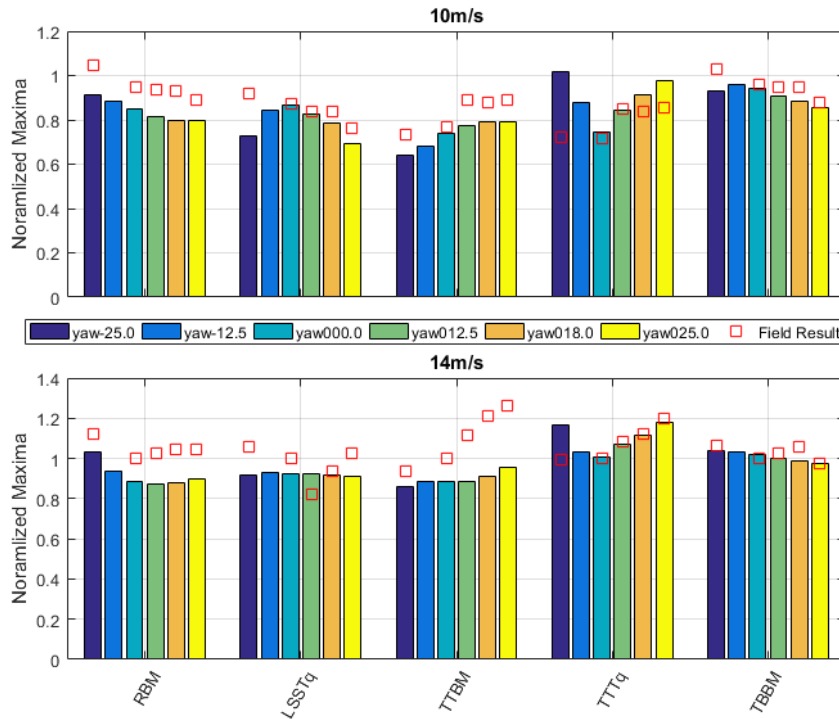
Figure 13. Comparison between predicted (FAST, bars) and measured (field, square symbols) mean extreme loads as a function of yaw offsets, for mean U_{hub}=10 m/s (top) and 14 m/s (bottom). The loads are normalized by their respective mean measured values at 0° yaw offset and U_{hub}=14 m/s.

Except for the tower-top resultant moment (which yielded a maximum relative error of 40% at 14-m/s wind speed), good
5 agreement exists between predicted and measured extreme loads.

For the RBM, the maximum values are seen at 14 m/s, where the mean values of the load peaks increase with nonzero yaw offsets, and with the largest values predicted and measured at γ=−25°. Note that the FAST underprediction of the loads is likely caused by the remaining difference in turbulence values between simulations and field data.

The LSSTq also shows the largest loads around rated wind speed, where both FAST and field data show limited to no effect
10 of yaw offset.

At tower top, a distinctive increase of peak TTBM with increasing yaw offset can be observed in Figure 13, and this trend persists in both the model and measured data. For the TTTq extremes, FAST predicts a minimum under aligned conditions, but field data show even smaller values at $\gamma=-25°$. Very good agreement exists for positive yaw offsets, however.

Finally, calculated TBBM extremes (highest values at 14-m/s wind speed) are seen to slightly decrease with increasing yaw offset. Whereas this trend is confirmed by the measurements at 10-m/s wind speed, at 14 m/s, the field data are noisier and show less influence of the yaw misalignment.

6   Conclusions

In this paper, we presented an analytical treatment, numerical investigations, and field data analyses to explore the effects of yaw offset operation on the loads of a commercial-grade wind turbine.

The results of models of increasing complexity were presented for the rotor aerodynamics under different yaw misalignments to shed some light on the physics and load predictions. It was shown that, under the presence of vertical wind shear, asymmetric conditions exist in the azimuthal distributions of the angle of attack and relative air velocity even under aligned inflow, which complicates the intuitive picture of the turbine response and might have further consequences on wake dynamics and control strategies. When turning the attention to the c_l distributions, rapid changes in values obtained under both steady and unsteady aerodynamics at the inboard sections of the blades were noted for wind speeds in power region 2.5, which are likely the responsible factors for the standard deviations noted in the blade-root FBMs. These effects were mostly attributed to the crossing of the stall region of the airfoil polars, which was seen as rather abrupt. At lower wind speeds (power region 2), these effects were partially eliminated by assuming rigid blades, thus demonstrating that, besides aerodynamics, the stiffness characteristics of the turbine play a significant role in the calculated DELs. A simple analytical model for the standard deviation of the out-of-plane component of the blade lift was presented and shown to be a valid proxy for DELs only under quasi-steady-state and rigid-rotor conditions. In fact, it was shown how stiffness characteristics and aerodynamics specific to the actual wind turbine model have a dominant role in the determination of the load statistics and therefore the fatigue response.

Furthermore, by considering more realistic turbulent wind fields, via both simulations and field data records, it was shown that the turbulence intensity distribution for the various mean wind-speed bins can significantly mask the effects caused by skewed inflow, and care must be taken to the actual site conditions to assess their effects on the loads. Only dedicated aero-servo-elastic simulations can capture the actual trends in loading as a function of yaw offset, and only if the proper turbulent inflow conditions are matched.

Aeroelastic simulations can do a good job predicting the blade-root FBM and EBM bending moment DELs, and it was shown how these, on average, exhibit different trends with yaw offsets. Whereas the FBM increased with nonzero misalignment, the EBM decreased with increasing yaw offsets. To assess the actual impact of misaligned operation on blade-root fatigue, the combined bending, or resultant moment, was analyzed via load roses. On average, the blade-root bending moment DEL decreased for positive yaw offsets and increased for negative offsets. Fairly large variations can be attributed to different turbulence seeds and data records, making generalization more difficult.

More complex trends were observed in shaft torque and tower-top bending moment DELs. For example, trend reversals in shaft torque from the simulation-derived data were noted when the wind speed increased toward power region 3. The initial DEL reduction with nonzero yaw offset seen for wind speeds below 10 m/s is replaced by a slight increase at higher wind speeds. Some of these effects are a direct consequence of the controller dynamics, and therefore difficult to generalize to multiple turbine models. The resultant moment DEL at tower top increased sharply with nonzero yaw offsets in the field-derived data, whereas the FAST predictions showed little or no influence of yaw misalignment.

Tower-top torque, which, together with the tower-top bending, can be responsible for the reliability of the yaw drive components, generally showed an increase in loading with positive misalignments, exhibiting good agreement between predictions and field measurements. To reiterate, however, standard deviations were fairly large and grossly dependent on turbulence characteristics, which tended to override the effects of yaw misalignment.

For the tower-base bending moment, the mean DELs derived from aeroelastic simulation decrease with positive yaw offsets, whereas measurement-derived data generally indicate a slight increase. Standard deviations of the predicted DELs are, however, quite large.

Extreme loads were also compared between field-measured and predicted values under operational conditions and skewed inflow. The results of the analysis showed that for the resultant moment at the blade root, an increase can occur under misaligned conditions. The shaft torque extreme load does not significantly change with nonzero yaw offsets. Tower-top bending moments increase with increasing yaw offset, whereas tower-top torque peaks increase with nonzero misalignment. At the tower base, the resultant bending moment tends to decrease slightly with increasing yaw error.

The current dichotomy between the desire of wind power plant production optimization and the conservatism toward reliability due to load increase concerns is corroborated by the results presented in this research. In contrast to what was reported in previous studies, the fatigue load components do not necessarily decrease with increasing yaw offsets, and we offered justifications as to why that might be happening. Whereas blade-root loads can be said to decrease, large standard deviations of the mean results also point to caution and to the need to carefully assess the site conditions. Even more attention should be paid to the yaw drive system, given the measured increase in tower-top extreme loads. The turbine controller, however, can significantly impact these results.

Future work should include an extension of the analysis to other types of turbines with different aerodynamics and elastic characteristics to further assess their impact on the results.

Appendix A: Fatigue Load Comparisons

Figures in Appendix A portray comparisons between predicted (FAST) and measured (field) DELs as a function of yaw offsets for mean hub-height wind speeds of 10 and 14 m/s. DELs are normalized by the mean measured value at 0° yaw offset. The error bars represent ±1 standard deviations.
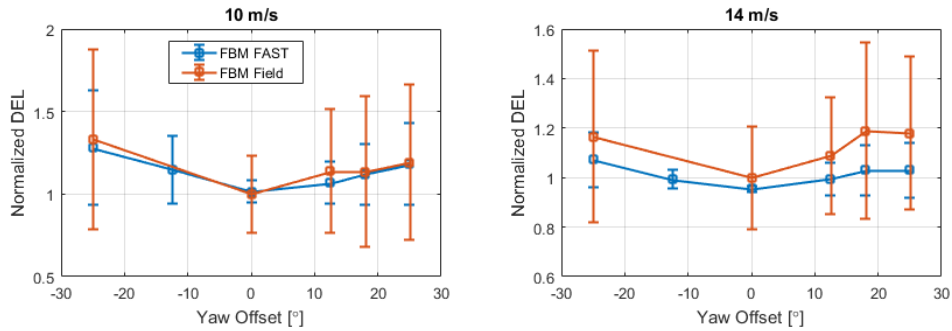
Figure A1. Comparison between predicted (FAST) and measured (field) FBM DELs.
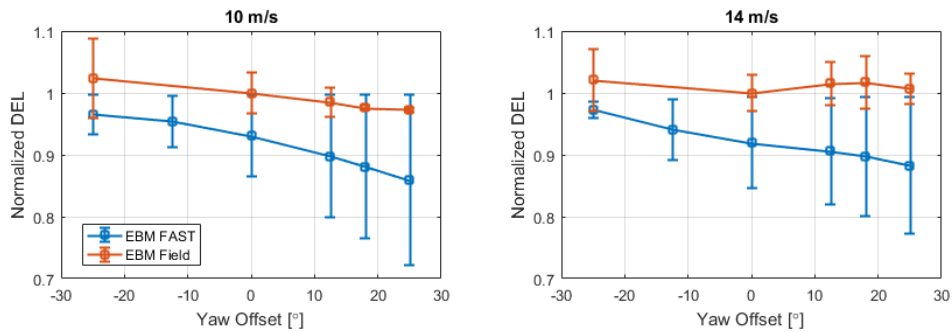
Figure A2. Comparison between predicted (FAST) and measured (field) EBM DELs.
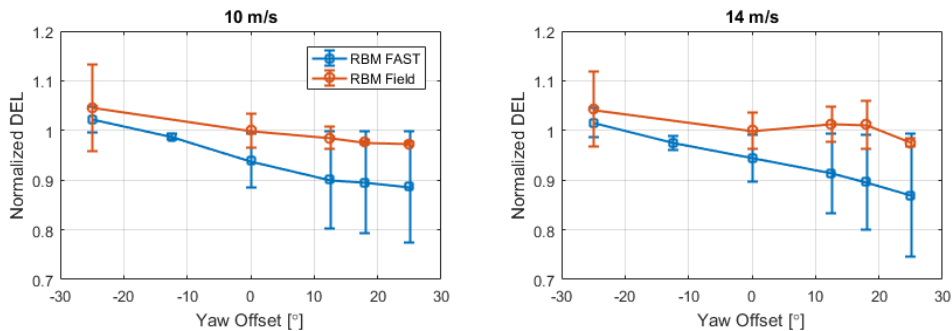
Figure A3. Comparison between predicted (FAST) and measured (field) RBM DELs. The largest component among eight load-rose sectors was selected for each yaw offset.
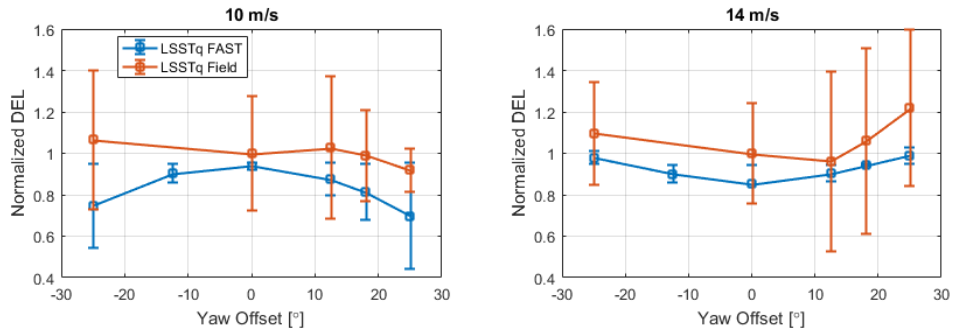
Figure A4. Comparison between predicted (FAST) and measured (field) LSSTq DELs.
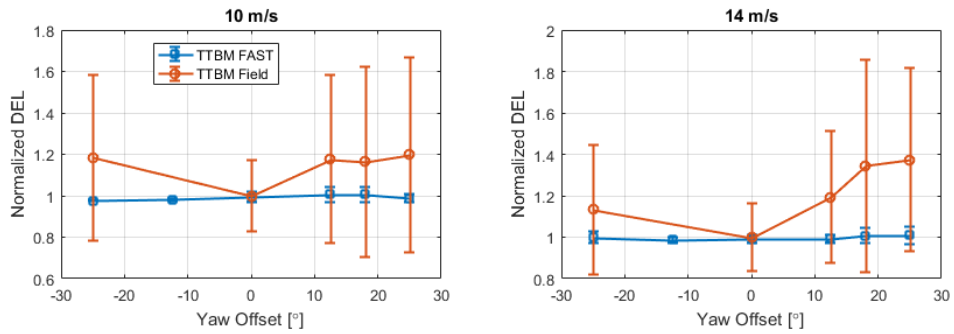
Figure A5. Comparison between predicted (FAST) and measured (field) TTBM DELs. The largest component among eight load-rose sectors was selected for each yaw offset.
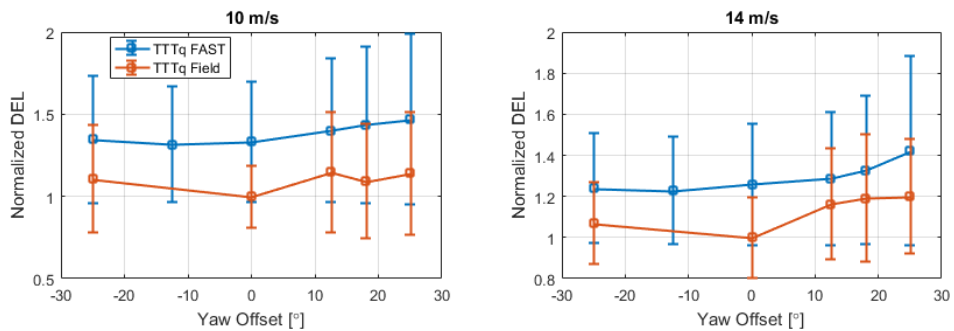
Figure A6. Comparison between predicted (FAST) and measured (field) TTTq DELs.
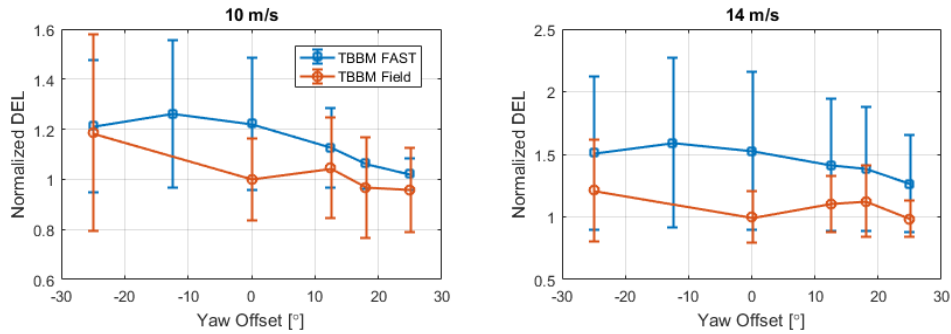
Figure A7. Comparison between predicted (FAST) and measured (field) TBBM DELs. The largest component among eight sectors was selected for each yaw offset.

Acknowledgements. Valuable suggestions for improving this paper came from Paul Veers and Jeroen van Dam. This work was supported by the U.S. Department of Energy under Contract No. DE-AC36-08GO28308 with the National Renewable Energy Laboratory. Funding for the work was provided by the DOE Office of Energy Efficiency and Renewable Energy, Wind Energy Technologies Office.

The U.S. Government retains and the publisher, by accepting the article for publication, acknowledges that the U.S. Government retains a

5   nonexclusive, paid-up, irrevocable, worldwide license to publish or reproduce the published form of this work, or allow others to do so, for U.S. Government purposes

References

Annoni, J., Gebraad, P., Scholbrock, A., Fleming, P., and Van Wingerden, J.: Analysis of axial-induction-based wind plant control using an engineering and a high-order wind plant model, Wind Energy, 19, 1135–1150, 2016.

Boorsma, K.: Power and loads for wind turbines in yawed conditions — Analysis of field measurements and aerodynamic predictions, Tech.
5 Rep. ECN-E–12-047, Energy Research Center of the Netherlands, The Netherlands, 2012.

Dahlberg, J. and Medici, D.: Potential improvement of wind turbine array efficiency by active wake control, in: Proceedings of European Wind Energy Conference, pp. 65–84, Madrid, Spain, 2003.

Damiani, R., Hayman, G., and Jonkman, J.: Development and Validation of a New Unsteady Airfoil Aerodynamics Model Within AeroDyn, in: 34th Wind Energy Symposium–SciTech 2016, AIAA, San Diego, CA, 2016.

10 Dana, S., Damiani, R., and Dykes, K.: Field Measurement Campaign of the GE 1.5-SLE under Yawed Inflow, Technical Report NREL/TP-5000-XXXXX, NREL, Golden, CO, 2017-forthcoming.

Downing, S. D. and Socie, D. F.: Simple rainflow counting algorithms, International Journal of Fatigue, 4, 31–40, 1982.

Fleming, P., Scholbrock, A., Jehu, A., Davoust, S., Osler, E., Wright, A., and Clifton, A.: Field-test results using a nacelle-mounted lidar for improving wind turbine power capture by reducing yaw misalignment, Journal of Physics: Conference Series, 524, 012 002,
15 doi:10.1088/1742-6596/524/1/012002, 2014.

Fleming, P., Gebraad, P. M. O., Lee, S., van Wingerden, J., Johnson, K., Churchfield, M., Michalakes, J., Spalart, P., and Moriarty, P.: Simulation comparison of wake mitigation control strategies for a two-turbine case, Wind Energy, 18, 2135–2143, 2015.

Frishman, F.: A Modern Course on Statistical Distributions in Scientific Work: Volume 1 — Models and Structures Proceedings of the NATO Advanced Study Institute held at the University of Calgary, Calgary, Alberta, Canada July 29 – August 10, 1974, chap. On the Arithmetic
20 Means and Variances of Products and Ratios of Random Variables, pp. 401–406, Springer Netherlands, Dordrecht, doi:10.1007/978-94-010-1842-5_32, 1975.

Gebraad, P. M. O., Teeuwisse, F. W., van Wingerden, J. W., Fleming, P. A., Ruben, S. D., Marden, J. R., and Pao, L. Y.: Wind plant power optimization through yaw control using a parametric model for wake effects — a CFD simulation study, Wind Energy, 19, 95–114, 2016.

Hand, M. M., Simms, D. A., Fingersh, L. J., Jager, D. W., Cotrell, J. R., Schreck, S., and Larwood, S. M.: Unsteady Aerodynamics Experiment
25 Phase VI: Wind Tunnel Test Configurations and Available Data Campaigns, Tech. Rep. NREL/TP-500-29955, National Renewable Energy Laboratory, Golden, CO, contract No. DE-AC36-99-GO10337, 2001.

IEC: 61400-1. Wind turbines—Part 1: Design requirements, 2005.

IEC: 61400-13:2015 Wind turbines — Part 13: Measurement of mechanical loads, 2015.

IEC: 61400-12-1:2017 Wind energy generation systems — Part 12-1: Power performance measurements of electricity producing wind
30 turbines, 2017.

Jiménez, A., Crespo, A., and Migoya, E.: Application of a LES technique to characterize the wake deflection of a wind turbine in yaw, Wind Energy, 13, 559–572, 2010.

Jonkman, J. M., Hayman, G. J., Jonkman, B. J., and Damiani, R. R.: AeroDyn v15 User's Guide and Theory Manual, Tech. rep., National Renewable Energy Laboratory, Golden, CO, 2015.

35 Kragh, K. A. and Hansen, M. H.: Load Alleviation of wind turbines by yaw misalignment, Wind Energy, 17, 971–982, doi:10.1002/we.1612, 2014.

Kragh, K. A. and Hansen, M. H.: Potential of power gain with improved yaw alignment, Wind Energy, 18, 979–989, doi:10.1002/we.1612, 2015.

Mendoza, I., Hur, J., Thao, S., and Curtis, A.: Power Performance Test Report for the U.S. Department of Energy 1.5-Megawatt Wind Turbine., Tech. Rep. TP-5000-63684, NREL, Golden, CO, 2015.

5 Mortimer, A.: New ideas for improving wind-farm outputs, Windpower Engineering & Development, pp. 46–50, 2016.

Ning, S. A., Hayman, G., Damiani, R., and Jonkman, J.: Development and Validation of a New Blade Element Momentum Skewed-Wake Model within AeroDyn, in: AIAA SciTech 2015 – 33rd Wind Energy Symposium, AIAA, Kissimmee, FL, doi:10.2514/6.2015-0215, 2015.

Schepers, J.: Annexlyse: Validation of Yaw Model, on Basis of Detailed Aerodynamic Measurements on Wind Turine Blades, Tech. Rep.
10 ECN-C-04-097, Energy Research Center of the Netherlands, The Netherlands, 2004.

Schepers, J.: Engineering models in wind energy aerodynamics: Development, implementation and analysis using dedicated aerodynamic measurements, Ph.D. thesis, TU Delft, The Netherlands, doi:10.4233/uuid:92123c07-cc12-4945-973f-103bd744ec87, 2012.

Schepers, J., Boorsma, K., and et al.: Final report of IEA Task 29, Mexnext (Phase 1) — Analysis of Mexico wind tunnel measurements, Tech. Rep. ECN-E–12-004, Energy Center of the Netherlands, 2011.

15 Schreck, S. J. and Schepers, J.: Unconventional Rotor Power Response to Yaw Error Variations, Journal of Physics: Conference Series, 555, 012 001, doi:10.1088/1742-6596/555/1/012001, 2014.

Vollmer, L., Steinfeld, G., Heinemann, D., and Kühn, M.: Estimating the wake deflection downstream of a wind turbine in different atmospheric stabilities: An LES study, Wind Energy Science, in open discussion, doi:10.5194/wes-2016-4, 2016.

Wagenaar, J., Machielse, L., and Schepers, J.: Controlling wind in ECN's scaled wind farm, in: Proceedings of the EWEA Annual Meeting,
20 Copenhagen, Denmark, 2012.

Zalkind, D. S. and Pao, L. Y.: The Fatigue Loading Effects of Yaw Control for Wind Plants, in: 2016 American Control Conference, pp. 537–542, ACC, Boston Marriot Copley Place, Boston, MA, 2016.